Electronic Supplementary Information

Bromine-bridged Dy_2 single-molecule magnet: magnetic anisotropy driven by *cis/trans* stereoisomers

Min Li,‡[a] Haipeng Wu,‡[a] Zhengqiang Xia,*[a] Vincent Montigaud,[b] Olivier Cador,[b] Boris Le Guennic,*[b] Hongshan Ke,[a] Wenyuan Wang,*[a] Gang Xie[a] and Sanping Chen*[a]

[a] *Key Laboratory of Synthetic and Natural Functional Molecule Chemistry of Ministry of Education, College of Chemistry and Materials Science, Northwest University, Xi'an, 710127, China*

E-mail: northwindy@126.com, wangwy@nwu.edu.cn, sanpingchen@126.com.

[b] *Univ Rennes, CNRS, ISCR (Institut des Sciences Chimiques de Rennes) –UMR 6226, F-35000 Rennes, France*

E-mail: boris.leguennic@univ-rennes1.fr.

‡ *These authors contributed equally to this work.*

Contents

1. Experimental Details

Materials and measurements. All experiments and manipulations were carried out under a dry nitrogen atmosphere using the standard Schlenk techniques or in a glovebox. Toluene was dried with over sodium under nitrogen atmosphere and distilled twice before use. Hexane was purchased from Adamas, distilled over sodium hydride and subsequently stored over 3 Å activated molecular sieves. Anhydrous $LnBr_3$ and Tricyclohexylphosphine oxide (Cy_3PO) were purchased from Alfa Aesar. Elemental analysis (C, H, N) was measured with 0.05 mL tin-capsules on a Perkin-Elmer 2400 CHN elemental analyzer. The samples of magnetic measurements were prepared in the glovebox by loading the samples with multiple recrystallization in an NMR tube and were restrained in eicosane. The samples were then placed under vacuum and flame-sealed. Magnetic susceptibility measurements were recorded using a Quantum Design MPMS-XL7 SQUID magnetometer with 1000 Oe applied field in the temperature range of 2-300 K. Alternating-current (ac) measurements were performed on the same magnetometer at ac frequencies ranging from 1 to 1500 Hz using a 2.0 Oe oscillating ac field. The measured susceptibilities were corrected for the diamagnetism of the constituent atoms and gelatin capsule by using tabulated Pascal constants and the blank sample holders.

Synthesis of $[Dy(Cy_3PO)_2(\mu\text{-}Br)(Br)_2]_2\cdot 2C_7H_8$ (Dy_2). A mixture of Cy_3PO (0.296 g, 1 mmol) and anhydrous $DyBr_3$ (0.201 g, 0.5 mmol) was dissolved in toluene (20 mL). The reaction mixture was stirred at 60℃ for 12 h. All the volatiles were removed under reduced pressure and the residue was extracted with hexane (*ca.* 20 mL). Subsequently, the insoluble residue was extracted with toluene (30 mL) and the extract filtered, concentrated and stored at -20 °C freezer overnight afforded colorless crystals of **Dy_2** (0.374 g, 72%). Anal. calcd: C, 47.51; H, 6.86. Found: C, 47.86; H, 6.98.

Synthesis of $[Gd(Cy_3PO)_2(\mu\text{-}Br)(Br)_2]_2\cdot 2C_7H_8$ (Gd_2). Complex **Gd_2** was prepared by analogous method from **Dy_2**, replacing $DyBr_3$ with $GdBr_3$ as starting metal bromide (0.429 g, 81%). Anal. calcd: C, 47.74; H, 6.89. Found: C, 47.97; H, 7.06.

2. Crystal Data and Structures

X-ray Single-Crystal Diffraction Analysis. Single-crystal X-ray data for **Dy_2** and **Gd_2** were collected at 170 K using an Oxford Cryosystems Cobra low-temperature device on a Bruker Smart Apex CCD diffractometer with a graphite-monochromatized Mo Kα radiation (λ = 0.71073 Å). Cell determination and data reduction were processed with the SAINT processing program.[1] The

absorption correction based on multiscan was applied in SADABS.[2] By using Olex2,[3] the structures were solved by direct methods with SHELXT and refined by full-matrix least-squares techniques against F^2 using SHELXL-2014 programs.[4] The SQUEEZE subroutine of the PLATON software was used to remove the scattering from the highly disordered solvent molecules.[5] The resulting new HKL files were used to further refine the structures. All non-hydrogen atoms were refined anisotropically. All hydrogen atoms were placed in calculated positions and refined isotropically. The crystal data and structural refinement parameters are summarized in Table S1, while selected bond lengths and angles for **Dy_2** and **Gd_2** are listed in Tables S2. All details for **Dy_2** and **Gd_2** can be found in CCDC 1852215 and 1949391 that contains the supplementary crystallographic data for this paper.

Table S1. Crystal data and structure refinement summary for **Dy_2**.

	Dy_2	**Gd_2**
Empirical formula	$C_{86}H_{148}Br_6Dy_2O_4P_4$	$C_{86}H_{148}Br_6Gd_2O_4P_4$
Formula weight	2174.38	2163.88
Crystal system	Triclinic	Triclinic
Temperature (K)	170	170
Space group	$P\bar{1}$	$P\bar{1}$
a (Å)	13.4056(6)	13.453(5)
b (Å)	15.3549(6)	15.414(6)
c (Å)	24.7629(12)	24.917(10)
α (°)	91.038(2)	90.982(12)
β (°)	94.840(2)	94.971(12)
γ(°)	113.840(2)	113.756(11)
V (Å^3)	4638.1(4)	4704(3)
Z	2	2
D_c (g m^{-3})	1.557	1.528
μ (mm^{-1})	4.297	4.059
F (000)	2196	2188
Reflns collected/unique	123871/21374	66353/19017
R_{int}	0.0475	0.0499
GOF on F^2	1.013	1.143
R_1[a] [$I > 2\sigma(I)$]	0.0331	0.0456
wR_2[b] (all data)	0.0768	0.1176
CCDC	1852215	1949391

[a]$R_1 = \Sigma(|| F_o | - | F_c ||)/\Sigma| F_o |$. [b]$wR_2 = [\Sigma w(F_o^2 - F_c^2)^2/\Sigma w(F_o^2)^2]^{1/2}$.

Table S2. Shape analysis for the metal centers of **Dy_2** and **Gd_2**.

Dy_2	HP-6	PPY-6	OC-6	TPR-6	JPPY-6

Dy1	32.951	24.863	**1.921**	14.706	26.891
Dy2	33.149	26.734	**1.342**	14.260	30.189

Gd$_2$	HP-6	PPY-6	OC-6	TPR-6	JPPY-6
Gd1	32.801	24.289	**1.866**	14.083	26.408
Gd2	33.069	26.819	**1.365**	14.249	30.138

HP-6 (D_{6h}): Hexagon
PPY-6 (C_{5v}): Pentagonal pyramid
OC-6 (O_h): Octahedron
TPR-6 (D_{3h}): Trigonal prism
JPPY-6 (C_{5v}): Johnson pentagonal pyramid J2

Table S3. Selected bond lengths (Å) and bond angles (°) for **Dy$_2$** and **Gd$_2$**.

Dy$_2$

Dy1-Br3	2.9404(4)	Br2-Dy1-Br4	165.001(13)
Dy1-Br4	2.9505(4)	O1-Dy1-Br3	93.45(8)
Dy1-O2	2.195(2)	O1-Dy1-Br4	84.19(7)
Dy1-Br2	2.7374(4)	O1-Dy1-O2	170.84(10)
Dy1-O1	2.188(3)	O1-Dy1-Br2	94.55(7)
Dy1-Br1	2.7347(4)	O1-Dy1-Br1	88.26(8)
O3-Dy2	2.199(3)	Br1-Dy1-Br3	174.020(15)
Br3-Dy2	2.8733(4)	Br1-Dy1-Br4	95.584(15)
Br4-Dy2	2.8822(4)	Br1-Dy1-Br2	99.320(16)
Dy2-O4	2.194(2)	O3-Dy2-Br3	173.49(7)
Dy2-Br6	2.8142(4)	O3-Dy2-Br4	94.86(7)
Dy2-Br5	2.7719(5)	O3-Dy2-Br6	83.09(7)
Br3-Dy1-Br4	78.907(10)	O3-Dy2-Br5	91.42(7)
O2-Dy1-Br3	90.01(6)	Br3-Dy2-Br4	81.143(11)
O2-Dy1-Br4	88.16(7)	O4-Dy2-Br3	97.30(10)
O2-Dy1-Br2	94.14(7)	O4-Dy2-Br3	86.63(7)
O2-Dy1-Br1	87.47(6)	O4-Dy2-Br4	167.77(7)
Br2-Dy1-Br3	86.266(12)	O4-Dy2-Br6	88.91(7)
Br5-Dy2-Br3	93.738(15)	O4-Dy2-Br5	90.39(7)
Br5-Dy2-Br4	90.607(13)	Br6-Dy2-Br3	91.835(12)
Br5-Dy2-Br6	174.333(15)	Br6-Dy2-Br4	91.265(12)
Dy2-Br3-Dy1	100.128(12)	Dy2-Br4-Dy1	99.684(11)

Gd_2

Gd1-Br3	2.9805(13)	O2-Gd1-Br3	87.68(9)
Gd1-Br4	2.9678(11)	O2-Gd1-Br4	90.03(9)
Gd1-Br1	2.7663(12)	O2-Gd1-Br1	94.88(9)
Gd1-Br2	2.7604(11)	O2-Gd1-Br2	87.06(9)
Gd1-O2	2.251(3)	O1-Gd1-Br3	83.63(10)
Gd1-O1	2.241(4)	O1-Gd1-Br4	94.32(10)
Gd2-Br3	2.9144(11)	O1-Gd1-Br1	95.12(10)
Gd2-Br6	2.8581(11)	O1-Gd1-Br2	87.80(10)
Gd2-Br4	2.9161(13)	O1-Gd1-O2	169.35(13)
Gd2-Br5	2.8192(11)	Br5-Gd2-Br3	90.78(3)
Gd2-O4	2.225(3)	Br5-Gd2-Br6	174.44(2)
Gd2-O3	2.226(4)	Br5-Gd2-Br4	93.66(2)
Br4-Gd1-Br3	78.931(19)	O4-Gd2-Br3	167.60(9)
Br1-Gd1-Br3	164.671(19)	O4-Gd2-Br6	88.55(9)
Br1-Gd1-Br4	85.95(2)	O4-Gd2-Br4	86.76(9)
Br2-Gd1-Br3	96.37(2)	O4-Gd2-Br5	90.47(9)
Br2-Gd1-Br4	174.57(2)	O4-Gd2-O3	97.25(13)
Br2-Gd1-Br1	98.86(3)	O3-Gd2-Br3	95.04(9)
Br3-Gd2-Br4	80.852(19)	O3-Gd2-Br6	82.87(9)
Br6-Gd2-Br3	91.35(3)	O3-Gd2-Br4	173.18(9)
Br6-Gd2-Br4	91.75(2)	O3-Gd2-Br5	91.83(9)

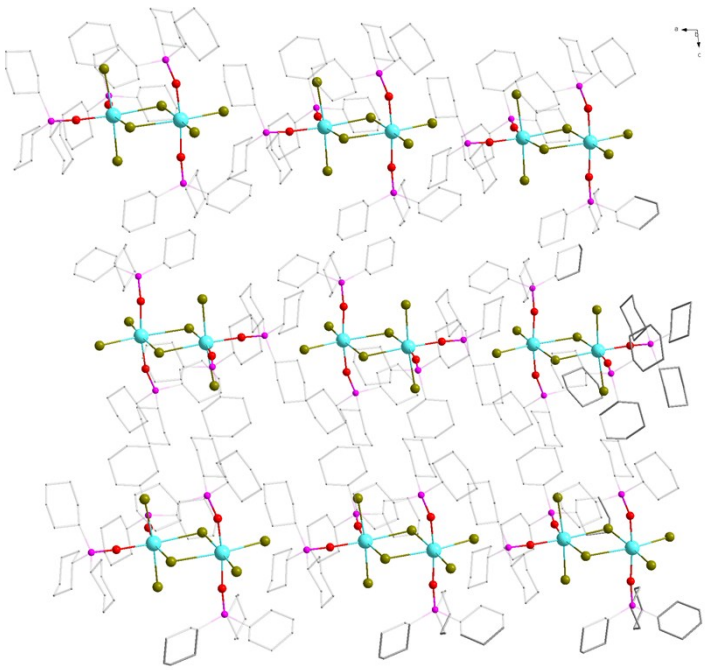

Fig. S1 The supramolecular network for **Dy_2**. Color codes: Dy, turquois; Br, dark yellow; P, pink; O, red; C, light grey.

3. Magnetic measurements

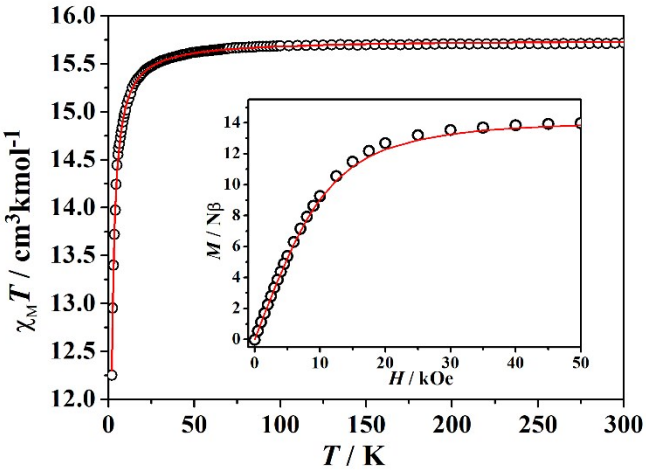

Fig. S2 Thermal evolution of the magnetic susceptibility and evolution of the magnetization with applied magnetic field at 2 K (inset) for **Gd$_2$**. The experimental values are represented as black dots while fitted data using J = -0.029 cm^{-1} are represented as red lines.

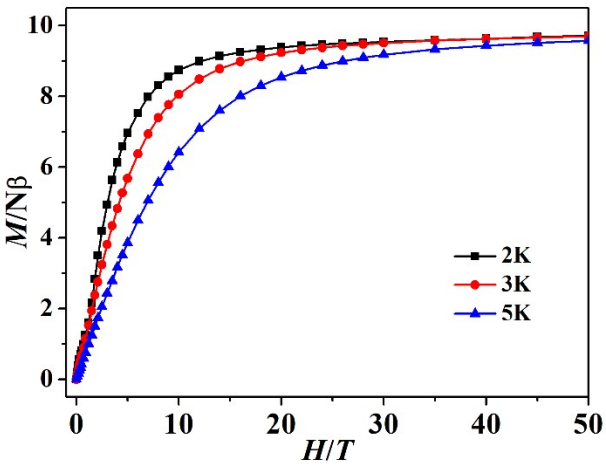

Fig. S3 Field dependent magnetizations from 0 to 50 kOe at 2, 3 and 5 K for **Dy$_2$**.

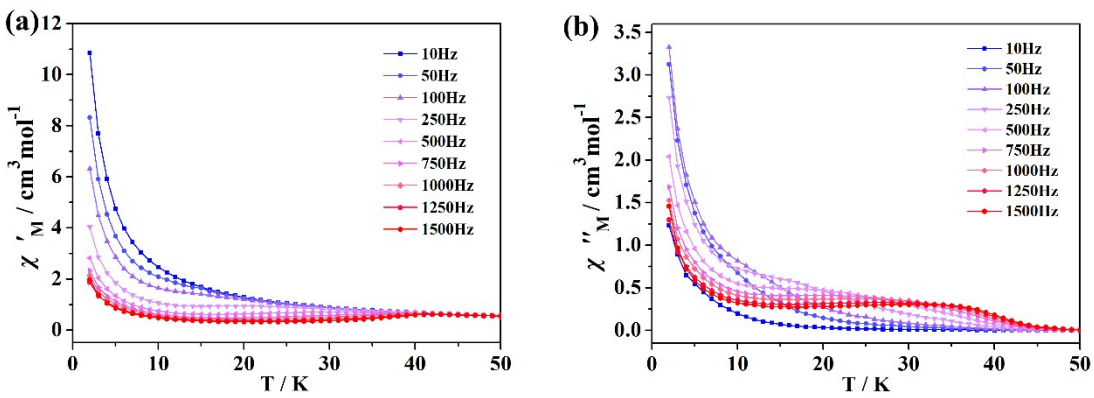

Fig. S4 Temperature-dependent in-phase χ' (a) and out-of-phase χ'' (b) ac susceptibility signals at the indicated frequencies under 0 Oe dc field for **Dy_2**.

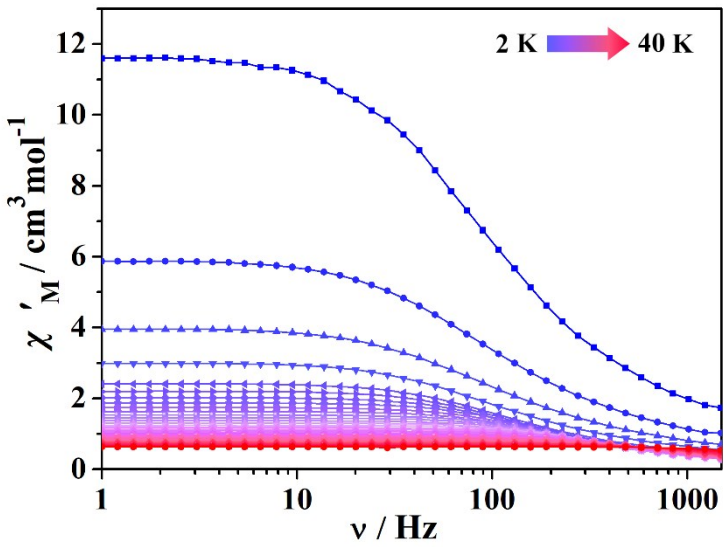

Fig. S5 Frequency-dependent in-phase χ' ac susceptibility signals for **Dy_2** at 0 Oe dc field.

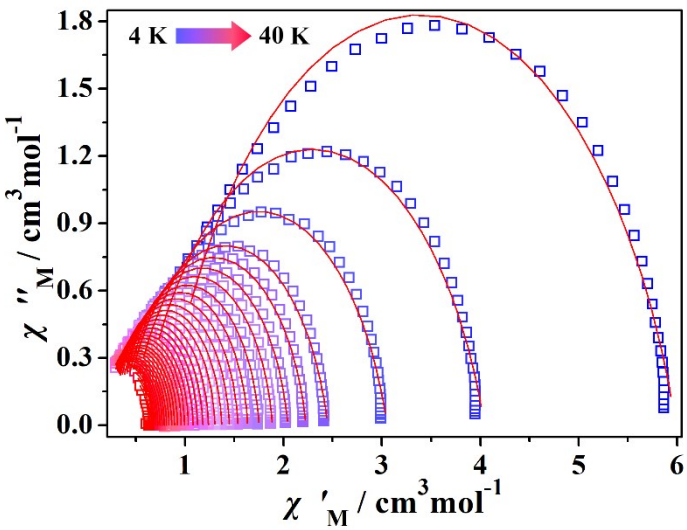

Fig. S6 Cole-Cole plots using the frequency-dependence ac susceptibility data under a 0 Oe dc field for **Dy_2**. The solid lines correspond to the best fits obtained with a generalized Debye model using CCFIT program.

Table S4. Best fitted parameters with a generalized Debye model under zero dc field for **Dy_2**.

T(K)	χ_S(cm^{3}mol^{-1})	χ_T(cm^{3}mol^{-1})	α	τ(s)

2	1.55118	11.7402	0.20322	0.00167
4	0.79188	5.98628	0.21745	0.00154
6	0.5452	4.041	0.2184	0.00146
8	0.44067	3.05144	0.19594	0.00135
10	0.37425	2.44843	0.16284	0.00116
11	0.35153	2.22906	0.14369	0.00106
12	0.32644	2.04531	0.12843	9.52214E-4
13	0.30983	1.88892	0.1088	8.55417E-4
14	0.28667	1.75418	0.10336	7.67041E-4
15	0.26924	1.63877	0.09142	7.12323E-4
16	0.2592	1.54006	0.07981	6.19392E-4
17	0.24081	1.45193	0.07403	5.55653E-4
18	0.23106	1.37415	0.06841	5.02265E-4
19	0.22521	1.30458	0.05876	4.56575E-4
20	0.21205	1.23908	0.05497	4.13549E-4
21	0.20564	1.18124	0.04951	3.9317E-4
22	0.19785	1.12893	0.04562	3.45147E-4
23	0.19399	1.08305	0.04239	3.15613E-4
24	0.18385	1.03575	0.03936	2.89777E-4
25	0.17349	0.99658	0.03746	2.77158E-4
26	0.17463	0.96218	0.03659	2.46164E-4
27	0.17303	0.92669	0.03454	2.28063E-4
28	0.16524	0.8948	0.03295	2.08799E-4
29	0.16864	0.8666	0.03038	1.95739E-4
30	0.16065	0.83888	0.02897	1.80689E-4
31	0.16743	0.81286	0.02191	1.69992E-4
32	0.16094	0.79142	0.03216	1.53389E-4
33	0.15917	0.76911	0.02534	1.41617E-4
34	0.15099	0.74608	0.02459	1.26094E-4
35	0.15483	0.72435	0.02332	1.13698E-4
36	0.15008	0.70376	0.01855	1.05243E-4
37	0.12544	0.68491	0.03163	8.51158E-5
38	0.14523	0.66628	0.02094	7.31992E-5
39	0.13408	0.65008	0.02918	5.8011E-5
40	0.17633	0.63338	0.01747	4.99785E-5

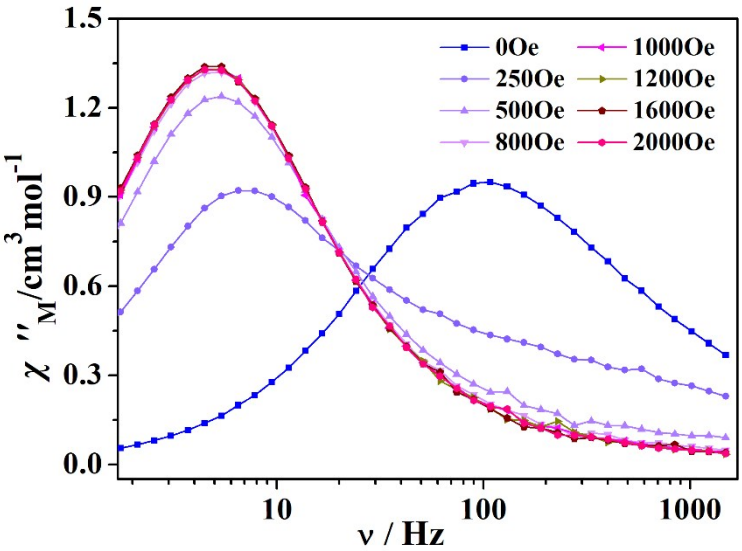

Fig. S7 Field dependence of out-of-phase χ'' ac susceptibility signals at 8 K for **Dy$_2$**.

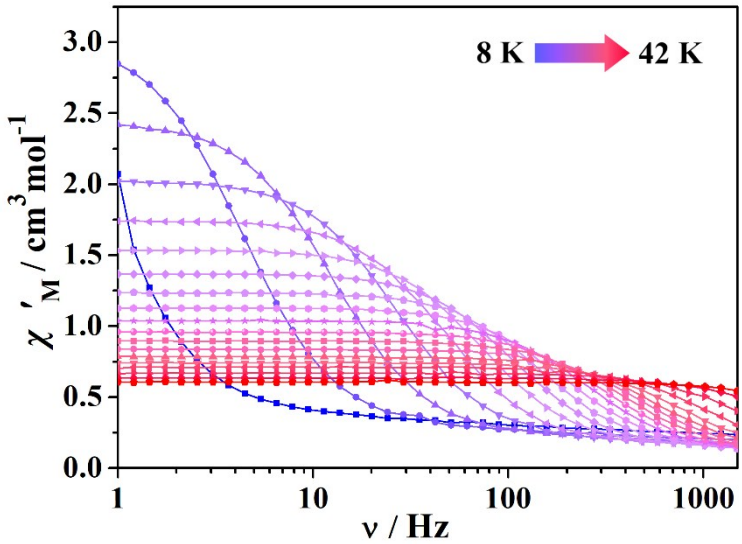

Fig. S8 Frequency dependence of the in-phase χ' ac susceptibility signals for **Dy$_2$** under 1000 Oe dc applied field.

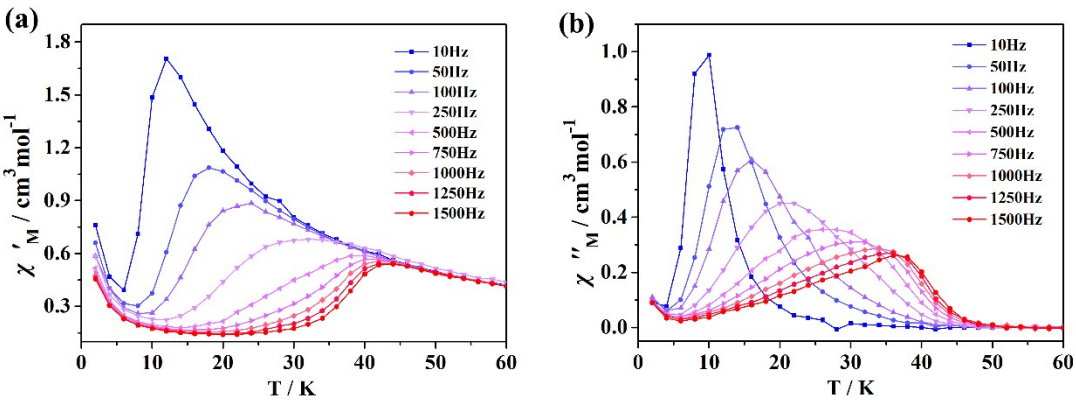

Fig. S9 Temperature-dependent in-phase χ' (a) and out-of-phase χ'' (b) ac susceptibility signals at the indicated frequencies under 1000 Oe dc field for **Dy₂**.

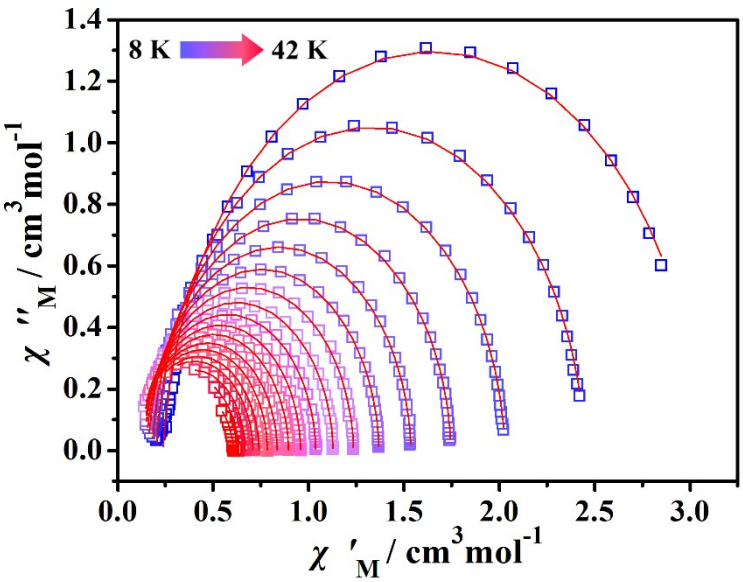

Fig. S10 Cole-Cole plots using the frequency-dependence ac susceptibility data under 1000Oe dc field for **Dy₂**. The solid lines correspond to the best fits obtained with a generalized Debye model using CCFIT program.

Table S5. Best fitted parameters with a generalized Debye model under 1000 Oe dc field for **Dy₂**.

T(K)	χ_S(cm^{3}mol^{-1})	χ_T(cm^{3}mol^{-1})	α	τ(s)
8	0.35423	2.99599	0.05308	0.03507
10	0.22527	2.40486	0.0428	0.01229
12	0.20095	2.00616	0.03476	0.00586
14	0.17905	1.7317	0.03241	0.00336
16	0.16717	1.52616	0.03142	0.00216
18	0.15445	1.36157	0.02937	0.00148
20	0.14655	1.23033	0.02709	0.00108

22	0.13895	1.12357	0.02978	8.20E-04
24	0.13149	1.03348	0.02827	6.35E-04
26	0.12794	0.95569	0.02604	5.06E-04
28	0.12792	0.89258	0.02375	4.12E-04
30	0.12384	0.83388	0.03286	3.38E-04
32	0.12108	0.78312	0.02395	2.74E-04
34	0.12433	0.73942	0.02788	2.17E-04
36	0.1284	0.70796	0.03701	1.60E-04
38	0.15133	0.6679	0.02105	1.10E-04
40	0.18651	0.6337	0.02002	6.95E-05
42	0.28238	0.60586	0.01914	5.09E-05

4. Theoretical calculations

Computational details

The atomic positions were extracted from the X-ray diffraction crystal structures. A calculation is performed on each Dy^{III} ion of **Dy_2** while the second Dy^{III} is replaced by a diamagnetic Y^{III} ion. All *ab-initio* calculations were performed using the State-Averaged Complete Active Space Self-Consistent Field approach with Restricted-Active-Space-State-Interaction method (SA-CASSCF/RASSI-SO), as implemented in the MOLCAS quantum-chemistry package (version 8.0).[6] In this approach, the relativistic effects are treated in two steps on the basis of the Douglas–Kroll Hamiltonian. The scalar terms are included in the basis-set generation and are used to determine the CASSCF wavefunctions and energies.[7] Spin-orbit coupling is then added within the RASSI-SO method, which mixes the calculated CASSCF wavefunctions.[8, 9] The resulting spin-orbit wavefunctions and energies are used to compute the magnetic properties and g-tensors of the ground state multiplet following the pseudospin $\tilde{S} = 1/2$ formalism, as implemented in the SINGLE_ANISO routine.[10] The resulting mononuclear fragments are then used to compute the anisotropic exchange interactions between the magnetic centers within the Lines model[11] with the software POLY_ANISO.[12,13] Cholesky decomposition of the bielectronic integrals was employed to save disk space and to speed up the calculations.[14]

The active space considered in the calculations consisted of the nine 4f electrons of the Dy^{III} ion, spanning the seven 4f orbitals; that is, CAS(9,7)SCF. State-averaged CASSCF calculations were performed for all of the sextets (21 roots), all of the quadruplets (224 roots) and 300 out of the 490

doublets of the Dy^{III} ion. Twenty-one sextets, 128 quadruplets and 107 doublets were mixed through spin–orbit coupling in RASSI-SO. All atoms were described with ANO-RCC basis sets with the following contractions [8s7p4d3f2g1h] for Dy; [7s6p4d2f1g] for Y; [6s5p3d2f] for the Br atoms; [4s3p2d] for the O atoms; [5s4p2d] for the P atoms; [2s1p] for the C atoms and [2s] for the H atoms.[15,16]

To give more insights on the orientation of the magnetic axis, the molecular electrostatic potential is calculated from the *ab-initio* LOPROP charge analysis[17] *(eq. 1)*.

$$V(r_i) = \sum_i^N \frac{q_i}{|r_i - r|} + \frac{p_i \cdot r_i}{|r_i - r|^3} + \frac{r_i \cdot (Q_i \times r_i)}{|r_i - r|^5} \qquad \textit{(eq. 1)}$$

where q_i, p, Q_i are respectively the charge, dipole and quadrupole moments of the i-th atom. The resulting molecular electrostatic potential is mapped and represented using the home-made CAMMEL code (Calculated Molecular Multipolar Electrostatics). The potential is drawn on a sphere defined by the user around the central lanthanide ion, for a given state (ground state in this case). For a clearer representation of the potential, the intensity can be directly related to both the color (red = high potential and blue = low potential) and the height of the irregularities. This program has already been used in previous works to give some hints on the orientation of magnetization axes.[18,19]

Table S6. Computed energy levels (the ground state is set at zero), composition of the *g*-tensor and decomposition of the wavefunction for each M_J state of the ground-state multiplet for Dy1 of **Dy_2**.

KD	Energy (cm^{-1})	g_X	g_Y	g_Z	Wavefunction composition*
1	0.0	0.00	0.00	19.87	100 % |±15/2>
2	312.1	0.02	0.02	17.02	100 % |±13/2>
3	558.9	0.80	0.98	13.47	91 % |±11/2>
4	647.4	2.12	6.07	13.31	71 % |±1/2> + 15 % |±9/2>
5	702.3	0.73	2.56	14.05	51 % |±3/2> + 19 % |±5/2> + 11 % |±9/2> + 10 % |±7/2>
6	736.6	9.20	6.30	0.24	53 % |±9/2> + 21 % |±3/2> + 15 % |±5/2>

7	780.5	0.16	5.19	12.09	44 % |±7/2> + 40 % |±5/2> + 13 % |±9/2>
8	819.3	0.99	2.07	17.67	41 % |±7/2> + 22 % |±5/2> + 15 % |±3/2> + 13 % |±1/2>

*Contributions < 10% are omitted.

Table S7. Computed energy levels (the ground state is set at zero) and compositon of *g*-tensor and decomposition of the wavefunction for each M_J state of the ground-state multiplet for Dy2 of **Dy_2**.

KD	Energy (cm^{-1})	g_X	g_Y	g_Z	Wavefunction composition*
1	0.0	0.06	0.75	18.70	90 % |±15/2>
2	38.1	0.23	0.69	17.73	31 % |±1/2> + 27 % |±3/2> + 18 % |±5/2>
3	99.0	1.95	2.89	16.12	36 % |±1/2> + 18 % |±3/2> + 17 % |±13/2> + 15 % |±5/2>
4	142.4	8.85	6.68	3.81	47 % |±13/2> + 22 % |±3/2> + 16 % |±1/2>
5	232.0	1.91	4.00	11.94	21 % |±13/2> + 19 % |±5/2> + 19 % |±11/2> + 19 % |±7/2> + 11 % |±9/2>
6	264.7	0.74	3.85	11.85	27 % |±9/2> + 26 % |±11/2> + 17 % |±7/2> + 11 % |±5/2>
7	291.7	2.04	5.37	12.46	33 % |±11/2> + 24 % |±5/2> + 14 % |±9/2> + 13% |±3/2>
8	352.8	0.24	0.78	18.22	38 % |±9/2> + 34 % |±7/2> + 10 % |±5/2>

*Contributions < 10% are omitted.

Table S8. Exchange spectrum (the first doublet is set at 0) and *g*-tensor main component (g_Z) resulting from the dipolar interaction for **Dy_2**.

KD	Relative E (cm^{-1})	g_Z

1	0.0	26.79
2	1.64	27.55

5. References

[1] Bruker, SMART, SAINT, and XPREP: Area Detector Control and Data Integration and Reduction Software, Bruker Analytical X-ray Instruments Inc., Madison, WI, 1995.

[2] G. M. Sheldrick, SADABS, Program for Empirical Absorption Correction, University of Göttingen, Göttingen, 1996.

[3] G. M. Sheldrick, *Acta Crystallogr. Sect. A,* 2008, **64**, 112.

[4] O. V. Dolomanov, L. J. Bourhis, R. J. Gildea, J. A. K. Howard, H. Puschmann, *J. Appl. Crystallogr.,* 2009, **42**, 339.

[5] A. Spek, *J. Appl. Crystallogr.,* 2003, **36**, 7.

[6] Aquilante, F.; Autschbach, J.; Carlson, R. K.; Chibotaru, L. F.; Delcey, M. G.; De Vico, L.; Galván, I. F.; Ferré, N.; Frutos, L. M.; Gagliardi, L.; Garavelli, M.; Giussani, A.; Hoyer, C. E.; Manni, G. L.; Lischka, H.; Ma, D. X.; Malmqvist, P.; Müller, T.; Nenov, A.; Olivucci, M.; Pedersen, T. B.; Peng, D. L. ; Plasser, F.; Pritchard, B.; Reiher, M. ; Rivalta, I.; Schapiro, I.; Segarra-Martí, J.; Stenrup, M.; Truhlar, D. G. ; Ungur, L.; Valentini, A.; Vancoillie, S.; Veryazov, V.; Vysotskiy, V. P.; Weingart, O.; Zapata, F.; Lindh, R. Molcas 8: New Capabilities for Multiconfigurational Quantum Chemical Calculations Across the Periodic Table. *J. Comput. Chem*. 2016, **37**, 506-541.

[7] Roos, B. O.; Taylor, P. R.; Siegbahn, P. E. M. A Complete Active Space SCF Method (CASSCF) Using a Density Matrix Formulated Super-CI Approach. *Chem. Phys.* 1980, **48**, 157-173.

[8] Malmqvist, P.Å.; Roos, B.O.; Schimmelpfennig, B. The Restricted Active Space (RAS) State Interaction Approach with Spin-Orbit Coupling. *Chem. Phys. Lett.* 2002, **357**, 230-240.

[9] Malmqvist, P.-Å.; Roos, B.O. The CASSCF State Interaction Method. *Chem. Phys. Lett.* 1989, **155**, 189–194.

[10] Chibotaru, L.F.; Ungur, L. *Ab Initio* Calculation of Anisotropic Magnetic Properties of

Complexes. I. Unique Definition of Pseudospin Hamiltonians and Their Derivation. *J. Chem. Phys.* 2012, **137**, 064112.

[11] Lines, M. E. Orbital angular momentum in the theory of paramagnetic clusters. *J. Chem. Phys.* 1971, **55**, 2977-2984.

[12] Chibotaru, L.; Ungur, L.; Soncini, A. The Origin of Nonmagnetic Kramers Doublets in the Ground State of Dysprosium Triangles: Evidence for a Toroidal Magnetic Moment. *Angew. Chem., Int. Ed.* 2008, **47**, 4126-4129.

[13] Ungur, L.; Van der Heuvel, W.; Chibotaru, L. Ab initio investigation of non-collinear magnetic structure and lowest magnetic excitations in dysprosium triangles *New J. Chem.,* 2009, **33**, 1224-1230.

[14] Aquilante, F.; Malmqvist, P.-Å.; Pedersen, T.B.; Ghosh, A.; Roos, B.O. Cholesky DecompositionBased Multiconfiguration Second-Order Perturbation Theory (CD-CASPT2): Application to the Spin State Energetics of Co^{III} (diiminato)(NPh). *J. Chem. Theory Comput.* 2008, **4**, 694-702.

[15] Roos, B. O.; Lindh, R.; Malmqvist, P. A.; Veryazov, V.; Widmark, P. O. Main Group Atoms and Dimers Studied with A New Relativistic ANO Basis Set. *J. Phys. Chem. A.* 2004, **108**, 2851-2858.

[16] Roos, B. O.; Lindh, R.; Malmqvist, P.; Veryazov, V.; Widmark, P. O.; Borin, A. C. New Relativistic Atomic Natural Orbital Basis Sets for Lanthanide Atoms with Applications to the Ce Diatom and LuF3. *J. Phys. Chem. A.* 2008, **112**, 11431-11435.

[17] Laura, G.; Roland, L.; Gunnar, K. Local properties of quantum chemical systems: The LoProp approach. *J. Chem. Phys.* 2004, **121**, 4494.

[18] Zhang, K.; Montigaud, V.; Cador, O.; Li, G.-P.; Le Guennic, B.; Tang, J.; Wang, Y.-Y. Tuning Magnetic Interactions in Dy(III)4 Single-Molecule Magnets. *Inorg. Chem.* 2018, **57**, 8550-8557.

[19] Huang, G.; Fernandez-Garcia, G.; Badiane, I.; Camarra, M.; Freslon, S.; Guillou, O.; Daiguebonne, C.; Totti, F.; Cador, O.; Guizouarn, T.; Le Guennic, B.; Bernot, K. Magnetic Slow Relaxation in a Metal–Organic Framework Made of Chains of Ferromagnetically Coupled SingleMolecule Magnets. *Chem. Eur. J.* 2018, **24**, 6983 –6991.